Front. Phys. 11(4), 114202 (2016)
DOI 10.1007/s11467-015-0543-4

RESEARCH ARTICLE

Quantitative analysis of lead in aqueous solutions by ultrasonic nebulizer assisted laser induced breakdown spectroscopy

Shi-Lei Zhong (钟石磊)[1,2], **Yuan Lu** (卢渊)[2], **Wei-Jin Kong** (孔伟金)[1], **Kai Cheng** (程凯)[2], **Ronger Zheng** (郑荣儿)[2,†]

[1] *College of Physics Science, Qingdao University, Qingdao 266071, China*
[2] *Optics and Optoelectronics Laboratory, Ocean University of China, Qingdao 266100, China*
Corresponding author. E-mail: †*rzheng@ouc.edu.cn*

Received July 22, 2015; accepted November 17, 2015

In this study, an ultrasonic nebulizer unit was established to improve the quantitative analysis ability of laser-induced breakdown spectroscopy (LIBS) for liquid samples detection, using solutions of the heavy metal element Pb as an example. An analytical procedure was designed to guarantee the stability and repeatability of the LIBS signal. A series of experiments were carried out strictly according to the procedure. The experimental parameters were optimized based on studies of the pulse energy influence and temporal evolution of the emission features. The plasma temperature and electron density were calculated to confirm the LTE state of the plasma. Normalizing the intensities by background was demonstrated to be an appropriate method in this work. The linear range of this system for Pb analysis was confirmed over a concentration range of 0–4,150ppm by measuring 12 samples with different concentrations. The correlation coefficient of the fitted calibration curve was as high as 99.94% in the linear range, and the LOD of Pb was confirmed as 2.93ppm. Concentration prediction experiments were performed on a further six samples. The excellent quantitative ability of the system was demonstrated by comparison of the real and predicted concentrations of the samples. The lowest relative error was 0.043% and the highest was no more than 7.1%.

Keywords laser-induced breakdown spectroscopy (LIBS), ultrasonic nebulizer, quantitative analysis, water solution, plasma diagnostics

PACS numbers 42.62.Fi, 52.38.-r

1 Introduction

The heavy metal element Pb is a common water pollutant in industrial wastewater and agricultural pesticide outflow. It is extremely harmful to the digestive system, nervous system, and immune system of human beings [1]. Strict restrictions on the concentration of Pb are laid down in waste water discharge standards [2] and water quality standards [3] worldwide. Therefore, scientific methods for the qualitative and quantitative analysis of Pb play an important role in the enforcement of those standards. Currently, the most common techniques used for Pb analysis include inductively coupled plasma mass spectrometry (ICP-MS) [4], inductively coupled plasma-atomic emission spectroscopy (ICP-AES) [5], and atomic absorption spectroscopy (AAS) [6]. However, each method has its own disadvantages, such as time-consuming operation, tedious sample preparation, and the use of additional harmful agents.

Laser induced breakdown spectroscopy (LIBS) is an atomic spectral analysis method that has drawn increasing attention in recent decades [7]. Many researchers have demonstrated that the LIBS method has immense potential in the field of solid sample analysis. However, many problems appear when the LIBS technology is applied to the analysis of liquid samples [8, 9]. On the one hand, the sensitivity of LIBS signals of bulk liquid samples is poor due to the low ablation efficiency and short plasma decay lifetime [8]. On the other hand, the quantitative analysis ability of the LIBS technique is considered as its heel of Achilles because of the complex matrix effect [10], and this situation becomes even worse for liquid

*Special Topic: The 1st Asian Symposium on Laser-induced Breakdown Spectroscopy (Eds.: Xiao-Yan Zeng, Zhe Wang & Yoshihiro Deguchi)

© Higher Education Press and Springer-Verlag Berlin Heidelberg 2016

sample applications. Therefore, various approaches have been taken to improve the signal sensitivity and stability for Pb analysis, such as moving the focus point onto the interface of the liquid and air [11], converting the liquid samples into solid ones [12], transforming bulk samples into flowing liquid jets [13], depositing the solute in samples on the surface of solid substrates [14, 15], and enriching the target elements on the exchange polymer membranes [16]. As a result, the obtained limits of detection (LOD) for Pb are usually lower than100 ppm.

Ultrasonic nebulizer (abbreviated as USN or UN) sample introduction units are also utilized in LIBS experiments to produce dry aerosol. Some of the studies are aimed at obtaining gaseous samples with a certain concentration of the target elements for gas analysis [17, 18], and the others aim to improve the LIBS signal in the analysis of liquid samples [19, 20]. For example, Hansheng et al. used a commercially available USN unit to produce dry gas aerosol, and then investigated the LIBS calibration techniques for analysis of the elements Cr and Cd in air [17]. Aras *et al.* combined a USN unit and a dryer unit into one system for LIBS analysis, which was utilized to analyze seven different metal elements in water, with an obtained LOD of 13.6 ppm for Pb [19]. The authors of this paper have developed a purpose-built USN unit which does not employ a dryer unit. The liquid droplets from this unit were directly broken down by the laser pulse to create plasma for LIBS analysis. The properties of the plasma such as the electron density, temperature, and spectral emission lifetime were experimentally investigated in the initial works. The LOD of manganese in water solution was subsequently confirmed as 0.242 ppm [20].

In this paper, the quantitative analysis ability of LIBS assisted by a USN unit for Pb detection was investigated. The repeatability, linear range, LOD, and accuracy of concentration prediction for Pb detection in water solutions are discussed with reference to the experimental results.

2 Experimental and operation procedure

Figure 1 illustrates the design of the experimental setup, which consists of a combination of a purpose-built ultrasonic nebulizer sampling unit and a conventional LIBS system.

2.1 Ultrasonic nebulizer sampling system

The ultrasonic nebulizer sampling system was composed of a sample cell and a buffer chamber. The glass sample cell was a hollow glass column with an oscillating plate

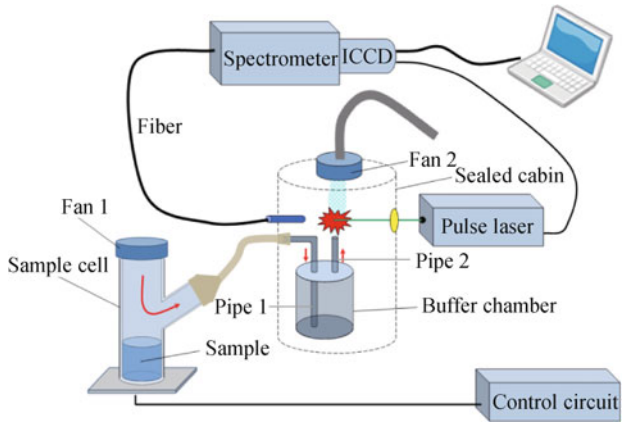

Fig. 1 Schematic diagram of the experimental setup.

fixed at the bottom with a fan (Fan 1) mounted on the top. A latex tube was used to connect the sample cell and the buffer chamber, which was a 20 mm high cylinder with an inside diameter of 12 mm. Two pipes (pipe 1 and pipe 2) with different lengths and same inside diameters (4 mm) were fixed to the top of the buffer chamber. One end of pipe 1 was connected to the latex tubing, and the other end was inserted into the chamber 10 mm above the base. The second pipe was also inserted into the chamber, with the inside end of the pipe 5 mm from the top side of the chamber.

When the USN unit was operating, the oscillating plate, driven by a capacitance feedback oscillator circuit, would vibrate at an ultrasonic frequency of 1.7 MHz to transform the liquid sample in the cell into a dense aerosol composed of liquid drops. Fan 1 then assisted the aerosol to flow slowly into the buffer chamber along pipe 1, and then slowly fill the inner space of the chamber from the bottom to the top. Finally, the aerosol would slowly and stably flow out of the buffer chamber through pipe 2. The aerosol flowing out of pipe 2 was maintained in a stable cylinder shape with the assistance of a second fan in order to facilitate LIBS analysis. The waste aerosol was gathered for treatment.

According to calculation formula proposed by Cáceres *et al.*, the average diameter of the droplets generated by USN depends on several factors including the vibration frequency, the surface tension of the liquid sample, atmosphere pressure, and temperature [21]. Using this formula, the average diameter of the droplets in this study was calculated as 2.92 μm. The experimental results revealed the transport efficiency to be approximately 400 mL/hour with a droplet density of 300 per mm^3.

2.2 LIBS System

The LIBS system utilized a Q-switch Nd:YAG laser (Quantel, Brilliant, 10 Hz repetition frequency, 8 ns pulse

width) operated at 1064 nm as the light source. The output laser pulses were focused on the aerosol generated by the USN unit using a quartz convex lens with a focal length of 38.1 mm. The resultant plasma light emission was collected by a convex fiber with one end placed about 2.5 cm away from the center of the plasma and the other end coupled into a Czerny–Turner spectrometer (Acton, Spectra Pro 2500i, 1200 lines/mm). The time resolved spectra were recorded with an ICCD (Andor, istar, DH734-18F) camera triggered by the Q-switch synchro-out signal.

2.3 Operational procedure

In order to obtain the most stable and repeatable LIBS signal, the operational procedure was elaborately designed and meticulously executed. Each set of valid data was obtained from independent experiments performed according to the procedure. In each experiment, 25 mL of liquid sample was injected into the sample cell and the capacitance feedback oscillator circuit was activated. After 20 s, a stable aerosol flow was achieved, the laser pulses were emitted. Each valid spectrum was an accumulation of the signals induced by 100 laser pulses. After each spectrum measurement, fan 1 continued operating for at least 60 s to purge the aerosol from the sample cell and the buffer chamber. The sample cell was then washed using deionized water twice. In order to correctly determine the calibration curves and concentration predictions, the data obtained from three independent experiments were used to calculate the average intensity and associated errors. The obtained spectral data were processed using the Origin software on a PC.

2.4 Sample preparation

The commercially available analytical reagent $Pb(NO_3)_2$ was dissolved into deionized water in a laboratory environment to prepare a high concentration aqueous sample. The low concentration samples were prepared by subsequent dilution operations.

3 Results and discussion

3.1 Parameter optimization

The temporal evolution features of spectral emission provide important information for parameter optimization in LIBS measurement. In this section, the experiments were performed using an aqueous solution with a concentration of 2072.0 ppm Pb. The spectral emissions emitted by the plasma, induced by 6 different laser pulse energies (38 mJ, 60 mJ, 81 mJ, 100 mJ, 120 mJ and 139 mJ), were recorded using the ICCD operating in the time resolved gate mode. For each pulse energy level, 12 spectra were measured with gate delays from 0.2 μs to 5.7 μs, and a gate width of 0.5 μs. The line of Pb at 220.35 nm was selected for the analysis, and the emission around this peak (200 pixels of the ICCD corresponding to a range of wavelength of 216.83 nm to 219.54 nm and 220.62 nm to 223.33 nm) was studied to provide measurements of the background. The obtained temporal evolution of intensity and signal to background ratio (SBR) is presented in Fig. 2.

As shown in Fig. 2(a), the intensity of Pb for all of the six pulse energies displayed a similar decreasing trend during the recorded period. The intensity decreased from the maximum to a very low value (about 5% of the max) over a time of approximately 4.2 μs, which indicated that the lifetime of the LIBS signal with this system could last for longer than several microseconds. Comparison of the curves obtained from the laser pulses of six different energies, revealed that the values did not change obviously in the recorded period when the laser pulse energies were higher than 81 mJ. The temporal evolutions of signal to background ratio are shown in Fig. 2(b). It can be seen that the values of the signal to background ratio in the initial period were not very high because of the contribution of the bremsstrahlung, which formed a strong

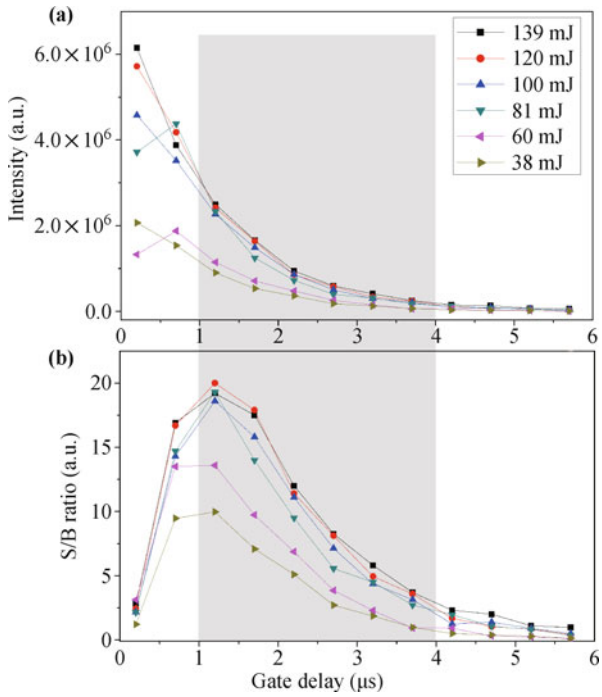

Fig. 2 Temporal evolutions of ion line intensity of lead at 220.35 nm **(a)** and signal to background ratio **(b)**.

background in the early stage of the plasma. The maximum signal to background ratios for different laser energies occur at different times. When the laser pulse energy was higher than 81 mJ, approximately 1.2 μs was required for the signal to background ratio to reach a maximum after the Q-switch signal arrived. For values of the gate delay time up to 4.2 μs, the signal to background ratio was higher than 1.7 for the energy of 120 mJ.

According to the above results, the laser energy was selected as 120 mJ. The gate delay and gate width employed were 0.5 μs and 4 μs as shown in Fig. 2. With the optimized experimental parameters, 30 independent experiments were carried out to analyze a solution sample with a Pb concentration of 2072 ppm. By subtracting the background from the original spectra, the absolute signal intensity of Pb at 220.35 nm was obtained, as shown in Fig. 3. Absolute signal to background ratios were also calculated to evaluate the stability and repeatability of the system.

As shown in Fig. 3, the RSD (Relative Standard Deviation) of the intensity obtained is 0.0033, and the RSD of the LIBS signal to background ratio is somewhat better than that of the intensity, reaching 0.0027. These results indicate that reproducibility of this system is acceptable. According to previous studies [11, 22], LIBS spectral lines of target elements could be normalized by the background emission, which is considered as an effective method for quantitative analysis, thus the same calibration method was utilized in this work.

3.2 Plasma temperature and electronic density

Local thermodynamic equilibrium (LTE) states of plasma are considered as one of the two necessary conditions for LIBS quantitative analysis. Therefore, the plasma temperature and electron density were calculated to understand the properties of the plasma induced in these experiments.

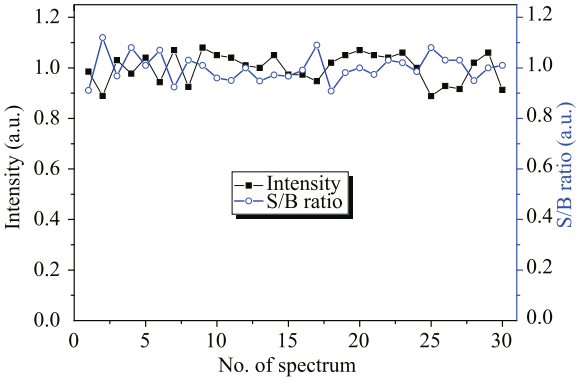

Fig. 3 Reproducibility ability of Pb II at 220.35 nm.

In order to obtain enough spectral lines, a sample of iron dissolved in water was employed for the plasma temperature calculations. Following the same experimental parameters employed previously, spectra of iron in ultrasonic nebulizer assisted LIBS experiments were obtained. 21 ion lines of iron were selected for Boltzmann Plot method. The intensities and parameters of those spectral lines are shown in Table 1.

By fitting the intensities of those 21 lines, a straight line was obtained as shown in Figure 4. The function of the line is shown below:

$$Y = -0.984x + 4.17.$$

The slope of the straight line obtained is –0.984 and the intercept is 4.17, with a correlation coefficient of 0.857. According the Boltzmann plot method, the slope of the straight line is equal to $-1/(KT)$, where the K is Boltzmann constant and T is the plasma temperature. Therefore, the plasma temperature under typical experimental conditions was determined to be 1.18×10^4 K.

The alpha line of hydrogen at 656.27 nm is often employed as an analytical tool for electron density calculation in LIBS investigations. In this work, this line was very strong and was selected for electron intensity calculation. The spectral dots obtained in the wavelength range from 645 nm to 665 nm are shown in Fig. 5.

As shown in Fig. 5, the Voigt profile fits the experimental data very well and the correlation coefficients obtained reached as high as 99.6%. The broadening of the obtained Lorentz profile was confirmed as 1.08 nm. According to Ref. [23], the electron density of hydrogen elements could be calculated by following formula.

$$N_{\mathrm{e}} = C(N_{\mathrm{e}}, T)(\Delta\lambda_{\mathrm{FWHM}})^{3/2},$$

where the constant $C(N_{\mathrm{e}}, T)$ is a coefficient which is

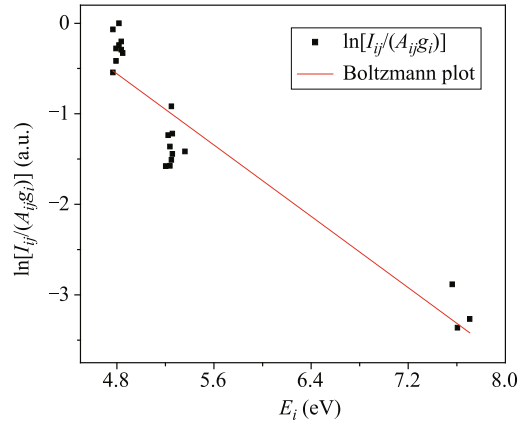

Fig. 4 Boltzmann plot of iron according experimental data of ultrasonic nebulizer assisted LIBS experiments.

Table 1 Parameters of the lines of iron used for Boltzmann plot.

No.	λ (nm)	I (10^7 a.u.)	g_i	A_{ij} ($10^8 S^{-1}$)	E_j (eV)	E_i (eV)	C_j	C_i	$\ln[I_{ij}/(A_{ij}g_i)]$ (a.u.)
1	235.91	7.28E+07	6	0.5	0.107	5.361	$3d^6(^5D)4s_{3/2}$	$3d^6(^5D)4p_{5/2}$	–1.41619
2	238.20	7.74E+08	12	3.13	0	5.203	$3d^6(^5D)4s_{9/2}$	$3d^6(^5D)4p_{11/2}$	–1.57957
3	238.86	1.74E+08	8	1.05	0.048	5.237	$3d^6(^5D)4s_{7/2}$	$3d^6(^5D)4p_{5/2}$	–1.57487
4	239.56	7.52E+08	10	2.59	0.048	5.222	$3d^6(^5D)4s_{7/2}$	$3d^6(^5D)4p_{9/2}$	–1.23676
5	239.92	1.84E+08	6	1.39	0.083	5.249	$3d^6(^5D)4s_{5/2}$	$3d^6(^5D)4p_{5/2}$	–1.50967
6	240.49	4.01E+08	8	1.96	0.083	5.237	$3d^6(^5D)4s_{5/2}$	$3d^6(^5D)4p_{5/2}$	–1.36336
7	240.67	1.90E+08	4	1.61	0.107	5.257	$3d^6(^5D)4s_{3/2}$	$3d^6(^5D)4p_{1/2}$	–1.21905
8	241.05	3.71E+08	6	1.55	0.107	5.249	$3d^6(^5D)4s_{3/2}$	$3d^6(^5D)4p_{5/2}$	–0.91883
9	241.33	9.64E+07	4	1.02	0.121	5.257	$3d^6(^5D)4s_{1/2}$	$3d^6(^5D)4p_{3/2}$	–1.44297
10	249.33	1.68E+08	16	3.04	2.635	7.606	$3d^6(^3H)4s_{13/2}$	$3d^6(^3H)4p_{15/2}$	–3.36387
11	258.59	4.69E+08	8	0.89	0	4.793	$3d^6(^5D)4s_{9/2}$	$3d^6(^5D)4p_{7/2}$	–0.41678
12	259.84	8.57E+08	6	1.43	0.048	4.818	$3d^6(^5D)4s_{7/2}$	$3d^6(^5D)4p_{5/2}$	–9.0E-04
13	259.94	1.36E+09	10	2.35	0	4.768	$3d^6(^5D)4s_{9/2}$	$3d^6(^5D)4p_{9/2}$	–0.54427
14	260.71	5.17E+08	4	1.73	0.083	4.837	$3d^6(^5D)4s_{5/2}$	$3d^6(^5D)4p_{3/2}$	–0.29214
15	261.19	7.27E+08	8	1.2	0.048	4.793	$3d^6(^5D)4s_{7/2}$	$3d^6(^5D)4p_{7/2}$	–0.27825
16	261.38	3.05E+08	2	2.12	0.107	4.849	$3d^6(^5D)4s_{3/2}$	$3d^6(^5D)4p_{1/2}$	–0.33002
17	261.76	2.31E+08	6	0.49	0.083	4.818	$3d^6(^5D)4s_{5/2}$	$3d^6(^5D)4p_{5/2}$	–0.24283
18	262.57	3.27E+08	10	0.35	0.048	4.768	$3d^6(^5D)4s_{7/2}$	$3d^6(^5D)4p_{9/2}$	–0.06802
19	262.83	2.84E+08	4	0.87	0.121	4.837	$3d^6(^5D)4s_{1/2}$	$3d^6(^5D)4p_{3/2}$	–0.20243
20	252.95	8.79E+07	10	2.2	2.807	7.707	$3d^6(^3F)4s_{7/2}$	$3d^6(^3F)4p_{9/2}$	–3.26645
21	253.68	1.97E+07	10	1.69	2.676	7.562	$3d^6(^3H)4s_{7/2}$	$3d^6(^3H)4p_{9/2}$	–2.88496

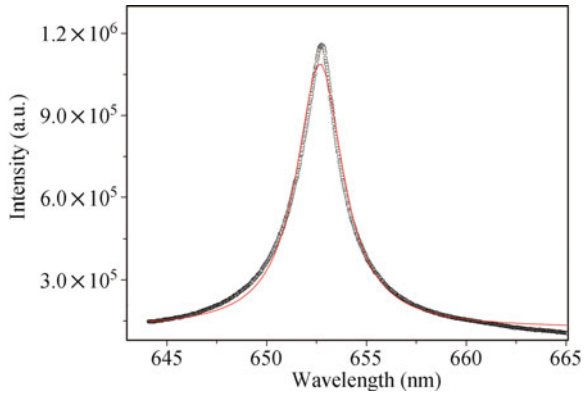

Fig. 5 The obtained alpha spectral line (○) of hydrogen and the fitting line (–) with Voigt profile.

weakly correlated with the electron density and temperature. The $\Delta\lambda_{FWHM}$ is the Stark broadening which could be regarded as Lorentz broadening obtained by fitting experimental data. The constant $C(N_e, T)$ can be found in Table 14-1 of Ref. [23]. Therefore, the electron density of the plasma in this study was determined to be 2.0×10^{17} cm^{-3}.

The criterion for LTE is that collisional processes must be much more important than radiative processes, which is possible at very high plasma electron densities such that:

$$N_e \geqslant 1.6 \times 10^{12} T^{1/2} \Delta E,$$

where the ΔE is the energy difference in electron volts between the two states of the transition of analytical element, and the T is the plasma temperature. In this study, the energy difference corresponding to the selected atomic line of Pb at 220.35 nm was 5.62 eV and the plasma temperature obtained was determined to be 1.18×10^4 K. Thus, the minimum electron density to guarantee a state of LTE could be confirmed as 2.67×10^{15} cm^{-3}, which were two orders of magnitude lower than the density obtained from the hydrogen spectrum in this study. Therefore it was reasonable to assume that the plasma induced with the optimized experimental parameters is in an LTE state.

3.3 Calibration curves and limits of detection

The variation of the signal intensity as a function of concentration is very important in LIBS experiments. On one hand, it reflects the features of the signal emission affected by self-absorption, which often occurs when the concentration increase to a certain extent. It is helpful to understand the radiation mechanism of plasma excited by a laser pulse. On the other hand, it is also the most important basis for determining the linear range of calibration. Pb in solution ranging from 25.9 ppm to 10 360 ppm were prepared and employed for LIBS experiments. The obtained results are shown in Fig. 6. The intensities

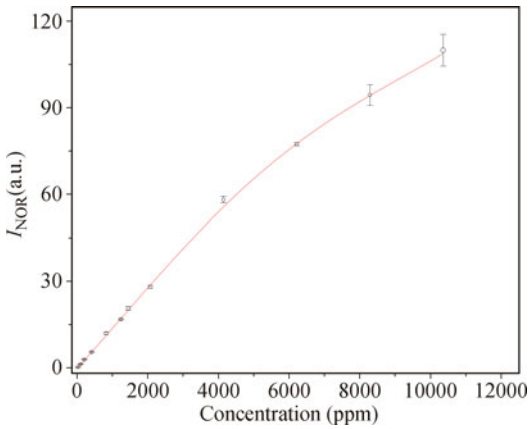

Fig. 6 Spectral intensities of Pb at 220.35 nm with concentration from 25.9 ppm to 10 360 ppm.

provided here were all separately normalized by the background for intensity calibration and are written as I_{NOR}.

As shown in Fig. 6, it could be found that the linearity between the spectral intensities and the concentrations of the Pb was acceptable for concentrations lower than 4000 ppm, however this relationship progressively deteriorated with further increases of concentration. This phenomenon is most likely because of the influence of self-absorption on the intensities, though no peak reverse was observed. This situation agrees with the Scheibe-Lomakin formula, which is expressed as $I = AC^b$, where I is the signal intensity of the target elements, C is the concentration of the element, A is a constant, and b is a variable which has a close relationship with the concentration. When the concentration is low enough the relationship shows a fine linearity and the value of b equals 1. However, when the concentration increases beyond a certain extent, the linear relationship is destroyed, and the value of b becomes less than 1. Therefore, in this study, the linear range could be confirmed as 0 ppm to approximately 4000 ppm.

The data displays excellent linearity between the normalized intensities and the concentrations in the linear range, and the obtained correlation coefficient of the fitted straight line was as high as 99.94%. The fitting line almost went through the origin of the coordinates as shown in the figure. The formula of the fitting line was

$$I_{\mathrm{NOR}} = 0.0139C - 0.226.$$

As shown in Fig. 7(b), the fitting results of the non-calibrated intensities obtained from the same set of samples display a lower correlation than those shown in Fig. 7(a), with a correlation coefficient of only 98.06%. There is an obvious difference of the error bars in the two figures, which proved the contribution of the normalization. In Table 1, spectral data of the samples in the linear

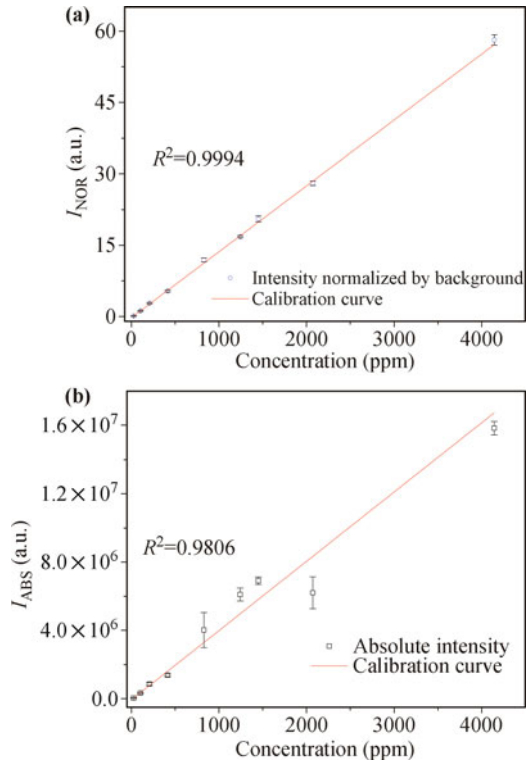

Fig. 7 Calibration curves of Pb with **(a)** and without **(b)** normalization by background.

concentration range was given to provide details of the experimental results. The average values of the absolute intensities of Pb, the backgrounds, and the normalized intensities were presented as $\overline{I}_{\mathrm{ABS}}$, $\overline{I}_{\mathrm{BCK}}$, and $\overline{I}_{\mathrm{NOR}}$, respectively.

When the sample concentration of Pb was 2072 ppm, the relative error of the original intensity of Pb was as high as 25.3%, however it could be improved to 0.21% by normalizing the absolute peak intensity by utilizing background. This demonstrates that intensity normalization by the background was an effective method for calibration curve improvement in this study.

The LOD of Pb could be calculated by the function below:

$$\mathrm{LOD} = 3\sigma/S,$$

where σ is the normalized standard deviation of the background, and S is the slope of the calibration curve. For the calculation of S, as mentioned above, the intensities employed the for calibration curve were all obtained from background-normalized spectral data. According to the calibration curve in Fig. 7(a), the value of S was confirmed as 0.0139. For the calculation of σ, 20 original spectral data sets were used for the standard deviation calculation, and an average background value of those 20 spectra was obtained. Through normalizing the standard

deviation by the average background value, the σ could be calculated which was then confirmed as 0.0135. The LOD value subsequently obtained was 2.93 ppm.

The LODs of Pb and some other common heavy metal elements obtained by this method are given in Table 3. The analytical line employed and the correlation coefficients are also provided. The LODs for heavy metal elements derived from this method are no more than several ppm, which is acceptable compared to other signal enhancing methods in the references.

3.4 Concentration prediction

In order to understand the quantitative prediction ability of the USN assisted LIBS method, 6 new samples were separately prepared. The concentrations of these samples ranged from 51.8 ppm to 2072.0 ppm as shown in Table 2. With exactly the same experimental procedure and spectral processing methods, the concentrations were predicted utilizing the previously developed expression. Every sample was independently measured 3 times, and the resulted plots (×) are shown in Fig. 8. The solid line in Figure 8 is the calibration curve obtained from Fig. 7(a).

Table 2 Spectra data of the employed samples in the linear range confirmed.

Concentration (ppm)	$\overline{I}_{\mathrm{ABS}}$ (a.u.)	$\overline{I}_{\mathrm{BCK}}$ (a.u.)	$\overline{I}_{\mathrm{NOR}}$ (a.u.)	Deviation (a.u.)
25.9	46100	363000	0.127	0.0367
103.6	336000	284000	1.19	0.102
207.2	870000	311000	2.80	0.13
414.4	1380000	257000	5.38	0.215
828.8	4020000	338000	11.90	0.407
1243.2	6110000	363000	16.80	0.217
1450.4	6910000	337000	20.50	0.624
2072.0	6210000	221000	28.00	0.468
4144.0	15800000	272000	58.10	1.10

Table 3 The LODs of common heavy metal elements in aqueous solutions got in this work versus the LODs got in other works.

Elements	This work			LODs in Refs.
	λ_{EM} (nm)	R^2	LOD (ppm)	
Pb	220.35	0.999	2.93	100 [11], 20 [12], 50 [13], 3.87 [14], 1.27 [15], 1.1 [16], 13.6 [19]
Cr	267.72	0.998	3.38	1.2 [12], 0.13 [16], 5.4 [19], 0.52 [15]
Cd	226.50	0.990	1.90	129 [12], 0.21 [16], 44.0 [19], 0.4 [15]
Mn[1)]	257.61	0.996	0.233	0.39 [24], 0.13 [15]
Zn[a]	206.19	0.996	0.596	120 [11], 21 [12], 0.85 [16], 41.6 [19], 0.51 [15]

[1)] The laser energy employed was 30 mJ.

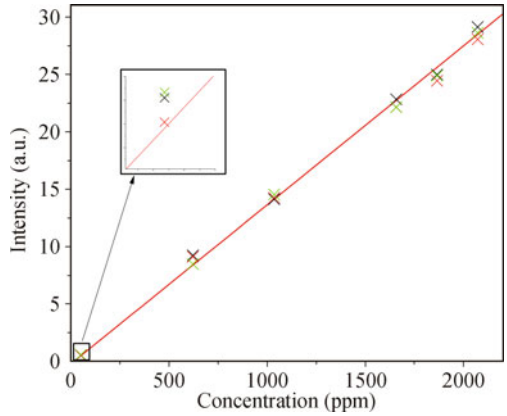

Fig. 8 The spectral intensities (×) of the 6 samples.

It can be seen that the plots for all the 6 samples match the calibration curve closely. According to the straight line fitted to the data, an expression for concentration prediction could be developed as below:

$$C_P = 16.3 + 72.2 I_{\mathrm{NOR}},$$

where C_P is the predicted concentration and I_{NOR} is the obtained intensity normalized by the background. The concentration could then be confirmed from the obtained spectra lintensities. The actual concentrations C, the concentrations predicted by independent intensities C_P, and the average values are presented in Table 4. The values of $\overline{C_P}$ were used to calculate the relative errors shown in Table 4. The actual concentrations (solid) and the average value of concentrations predicted (grid lines) of the 6 samples are presented in Fig. 9 in the form of a histogram.

It was found that the concentrations of the samples could be accurately predicted. The relative errors of the predicted concentration for all samples were lower than 7.1%. The average relative errors ($\overline{E_R}$) of the samples with lower concentration were obviously higher than those of the higher-concentration samples, which could reach 7.07% and 6.50%. The most accurate concentration prediction was obtained from the sample with a concentration of 2072.0 ppm, which has a low average relative error of 0.43%. This phenomenon satisfied the basic

Table 4 The predicted concentrations and its relative errors.

Sample	C (ppm)	C_P (ppm)			$\overline{C_P}$ (ppm)	$\overline{E_R}$
		1_{st}	2_{nd}	3_{rd}		
S_1	51.8	56.42	52.72	57.25	55.46	7.07%
S_2	621.6	682.8	674.9	628.4	662.0	6.50%
S_3	1036.0	1036	1045	1066	1049	1.25%
S_4	1657.6	1664	1615	1614	1631	1.60%
S_5	1864.8	1820	1782	1814	1805	3.20%
S_6	2072.0	2119	2041	2082	2081	0.43%

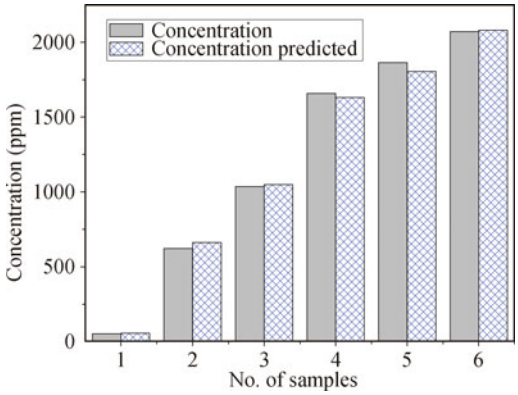

Fig. 9 The predicted concentration (*fill*) versus the real concentration (*grid line*) of the 6 samples.

tenets of analytical chemistry.

4 Conclusions

In this work, an ultrasonic nebulizer unit was established to introduce liquid samples for LIBS detection in order to improve the quantitative analysis ability of the heavy metal element Pb. An operational procedure was designed to guarantee the stability and repeatability of the LIBS signal. A series of experiments were carried out with optimized experimental parameters. The plasma temperature and electron density were calculated to confirm the LTE state of plasma. According to the experimental data obtained, normalizing the LIBS spectral intensity by background was demonstrated to be an applicable method to improve the calibration curves in this study. The linear range of this system for Pb analysis ranged between 0–4150 ppm and the correlation coefficient of the calibration curve was as high as 99.94%. The LOD of Pb and of 4 other heavy metal elements obtained utilizing this method were no more than several ppm. The excellent quantitative ability was demonstrated by comparing the real and predicted concentrations of samples. The relative error ranged from a low of 0.043% to a maximum of 7.1%.

Acknowledgements Financial support from the National Natural Science Foundation of China (Grant No. 11104153) is highly acknowledged.

References

1. B. He, Z. Yun, J. Shi, and G. Jiang, Research progress of heavy metal pollution in China: sources, analytical methods, status, and toxicity, *Chinese Science Bulletin* 58, 134 (2013)
2. MoEPot PRC, Integrated wastewater discharge standard (GB 8978-1996), 1996
3. G. Who, Guidelines for drinking-water quality, World Health Organization, 2011
4. D. V. Biller and K. W. Bruland, Analysis of Mn, Fe, Co, Ni, Cu, Zn, Cd, and Pb in seawater using the Nobias-chelate PA1 resin and magnetic sector inductively coupled plasma mass spectrometry (ICP-MS), *Marine Chemistry* 130, 12 (2012)
5. B. N. Kumar, D. Venkata Ramana, Y. Harinath, K. Seshaiah, and M. Wang, Separation and Preconcentration of Cd (II), Cu (II), Ni (II), and Pb (II) in Water and Food Samples Using Amberlite XAD-2 Functionalized with 3-(2-Nitrophenyl)-1 H-1, 2, 4-triazole-5 (4 H)-thione and Determination by Inductively Coupled Plasma–Atomic Emission Spectrometry, *J. Agricult. Food Chem.* 59, 11352 (2011)
6. S. Ayata, S. S. Bozkurt, and K. Ocakoglu, Separation and preconcentration of Pb (II) using ionic liquid-modified silica and its determination by flame atomic absorption spectrometry, *Talanta* 84, 212 (2011)
7. Z. Wang, T.-B. Yuan, Z.-Y. Hou, W.-D. Zhou, J.-D. Lu, H.-B. Ding, and X.-Y. Zeng, Laser-induced breakdown spectroscopy in China, *Front. Phys.* 9(4), 438 (2014)
8. A. De Giacomo, M. Dell'Aglio, O. De Pascale, and M. Capitelli, From single pulse to double pulse ns-laser induced breakdown spectroscopy under water: Elemental analysis of aqueous solutions and submerged solid samples, *Spectrochim. Acta Part B* 62, 721 (2007)
9. J.-S. Xiu, X.-S. Bai, V. Motto-Ros, and J. Yu, Characteristics of indirect laser-induced plasma from a thin film of oil on a metallic substrate, *Front. Phys.* 10(2), 104204 (2015)
10. D. W. Hahn and N. Omenetto, Laser-induced breakdown spectroscopy (LIBS) (I): Review of basic diagnostics and plasma–particle interactions: Still-challenging issues within the analytical plasma community, *Applied Spectroscopy* 64, 335A (2010)
11. P. Fichet, P. Mauchien, J.-F. Wagner, and C. Moulin, Quantitative elemental determination in water and oil by laser induced breakdown spectroscopy, *Analytica Chimica Acta* 429, 269 (2001)
12. D. D. Pace, C. D'Angelo, D. Bertuccelli, and G. Bertuccelli, Analysis of heavy metals in liquids using laser induced breakdown spectroscopy by liquid-to-solid matrix conversion, *Spectrochim. Acta Part B* 61, 929 (2006)
13. J. Wu, Y. Fu, Y. Li, Y. Lu, Z. Cui, and R. Zheng, Detection of metal ions in water solution by laser induced breakdown spectroscopy, *Spectroscopy and Spectral Analysis* 28, 1979 (2008)
14. J. Xiu, H. Hou, S. Zhong, Z. Wang, Y. Lu, and R. e. Zheng, Quantitative determination of heavy metal element Pb in aqueous solutions by laser-induced breakdown spectroscopy using paper slice substrates, *Chinese Journal of Lasers* 38, 0815003 (2011)
15. H. R. Griem, Plasma Spectroscopy, New York: McGraw-Hill, 1964, p. 1

16. N. E. Schmidt and S. R. Goode, Analysis of aqueous solutions by laser-induced breakdown spectroscopy of ion exchange membranes, *Applied Spectroscopy* 56, 370 (2002)
17. H. Zhang, F.-Y. Yueh, and J. P. Singh, Performance evaluation of laser-induced breakdown spectrometry as a multimetal continuous emission monitor, *J. Air Waste Manag. Assoc.*51, 681 (2001)
18. J. P. Singh, and S. N. Thakur, Laser-Induced Breakdown Spectroscopy, Elsevier, 2007
19. N. Aras, S. Ü. Yeşiller, D. A. Ateş, and Ş. Yalçın, Ultrasonic nebulization-sample introduction system for quantitative analysis of liquid samples by laser-induced breakdown spectroscopy, *Spectrochim. Acta Part B* 74, 87 (2012)
20. S. Zhong, Y. Lu, K. Cheng, and R.-E. Zheng, Ultrasonic nebulizer assisted LIBS for detection of trace metal elements dissolved in water,*Spectroscopy and Spectral Analysis* 31, 1458 (2011)
21. M. A. Tarr, G. Zhu, and R. F. Browner, Fundamental aerosol studies with an ultrasonic nebulizer, *Applied Spectroscopy* 45, 1424 (1991)
22. J. Cáceres, J. T. López, H. Telle, and A. G. Ureña, Quantitative analysis of trace metal ions in ice using laser-induced breakdown spectroscopy, *Spectrochim. Acta Part B* 56, 831 (2001)
23. H. R. Griem, High-density corrections in plasma spectroscopy, *Phys. Rev.* 128, 997 (1962)
24. V. Lazic, S. Jovicevic, R. Fantoni, and F. Colao, Underwater by an optimized laser excitation and its application for liquid analyses by laser-induced breakdown spectroscopy, *Spectrochim. Acta Part B* 62, 1433 (2007)